Journal homepage:
http://www.bsu.edu.eg/bsujournals/JVMR.aspx

Online ISSN: 2357-0520 Print ISSN: 2357-0512

Original Research Article

Radiologic, Ultrasonic and pathological assessments of locally applied Chitosan on promotion of experimentally induced tibial fracture healing in rats

Kotb, M. M. A[3].; Ragab, G. A.[1]; Fathy, M. Z.[1]; Haggag, U.[1] , and Nesreen. M. Safwat[2]

[1] Surgery, Anesthesiology and Radiology Department, Faculty of Veterinary Medicine, Beni-Suef Univ., Beni Suef, Egypt.
[2] Pathology Department, Faculty of Veterinary Medicine, Beni-Suef University, Beni Suef, Egypt.
[3] Veterinarian in Garado Veterinary Unit, El- Fayoum, Egypt.

ABSTRACT

The objective of the present study was to evaluate the ability of Chitosan to promote induced tibial fracture healing in a rat model. The study was conducted on 14 albino rats divided into two equal groups (seven rats in each group). The first group was considered as a control group. The second group was injected Chitosan solution 0.1 mg/kg into the fracture gap. The progress of healing in each group was evaluated by clinical, radiography, ultrasonography and pathological examinations. The healing process was observed to be superior in the Chitosan group compared to the control one. Chitosan was found to promote healing of injured bone and is suggested to be used in cases of complicated or delayed bone fracture.

ARTICLE INFO

Article history:

Received

12/8/2019

Accepted
19/11/2019

Online 1/2/2020

Keywords:

Albino rats, Fracture, Healing, Pathological, Radiological, Ultrasonic

[*]**Corresponding author:** Fathy, M. Z., Surgery, Anesthesiology and Radiology Department, Faculty of Veterinary Medicine, Beni-Suef Univ., Beni Suef, Egypt.
Email: Mzfhussein83@gmail.com

1. Introduction

The pharmacological stimulation of fracture healing gains more attention in clinical practice. Biomaterials are those non-living materials that used in medical, biomedical and other fields, aimed to react with the biological system such as chitosan which used as a functional stand by for tissues replacement, such as bone tissue. Also, they do not cause risks of disease transmission or immune rejection, as well as of low cost (Malafaya et al., 2007, Giannoudis et al., 2007, Spin-Neto et al., 2010, Ezoddini-Ardakani et al., 2011, Ruijin et al., 2016, Kmiec et al., 2017).

Rat fracture models are of major significance, they provide insights into bone metabolism of living organisms and potentially uncover positive or negative effects in the use of certain types of medication. Furthermore, they give the roads to investigate the physiological process of bone healing. (Prodinger et al., 2018).

Osteoblasts play critical roles in bone formation, chitosan can stimulate osteoblast proliferation and maturation (Levengood and Zhang, 2014, Ho et al., 2015 and Vasconcelos et al., 2018a) with minimum inflammatory response after implantation(Almeida et al., 2014). Therefore, Castillo et al. (2005) suggested the potential of chitosan scaffolds for therapy of bone diseases, including bone defects and bone fractures.

Plain radiography remains the most commonly used radiographic tool for assessing bone health and fracture healing. This is due to lower cost, wider availability, and lower radiation exposure of plain radiography compared to other available modalities (Davis et al., 2004).

Ultrasonography could be used to record fracture healing steps earlier than traditional radiography in long bone fractures pets. The criteria for diagnosing of fracture healing are echogenicity of the structure and the surface of the fractured bone and its callus. The image of the callus progressively becomes hyperechoic with its structure changing from homogeneous (fresh hematoma) to inhomogeneous, and then to homogeneous again with mature callus formation (Caruso et al., 2000).

2. Materials and Methods

The present study was enrolled on 18 healthy male albino rats having a weight 172.71 ± 4.32 gm randomly allocated into two groups {control (C G) and chitosan (CT G)}, nine rats in each and housed in cages with solid floors covered with 3cm of soft bedding (hay) and reared on standard diet daily with continuous available water for 24 hour. The experimental study was carried out after 7 days of acclimatization for the rats with the standard protocol of 12 hour light and dark and of each group in its specific metal cage. These animals were housed under standard environmental conditions. Rats were obtained from lab animal unit; Department of Physiology, Faculty of Veterinary Medicine, Beni-Suef University, Egypt. Rats were kept in standard laboratory conditions 22±3°C, 60±5% humidity and a 12 hours light/dark cycle. Animal handling was carried out in accordance with and approved by the institutional animal care and use committee, Faculty of Veterinary Medicine, Beni-Suef University

The shrimp (*M. monoceros*) shells were obtained fresh from the shrimp market in Fayoum. Prior to use, 250 grams of shrimp shells were washed thoroughly with distilled water and then cooked 20 min at 100°C. The solid material obtained was dried, minced to obtain a fine powder according to the method described by Jellouli et al. (2008).

Each rat was injected 100 mg/kg ketamine (2 ml) (Ketamine® 5% sol. Sigma-Aldrich Co.); plus 10/kg mg xylazine hydrochloride (2 ml) (Xyla-ject® ADWIA Co. A.R.E) 0.7 ml of the mixture was injected intra-peritoneal by using syringe 23-25 gauge 5/8 inch needle (Flecknell, 2015 and Hohlbaum et al., 2018)

Tibiae fracture induced by bending the lower part against an artery forceps which applied externally, the fractures were confirmed

radiographically according to (Handool et al. 2018) and external fixation retained by casting tape.

The first group was left as control (CG) and in the second group Chitosan (CT G); tibiae was locally injected by a single dose 10 % of Chitosan solution at the side of fracture according to (Kolios et al., 2010). (Fig. 1 and Fig. 2).

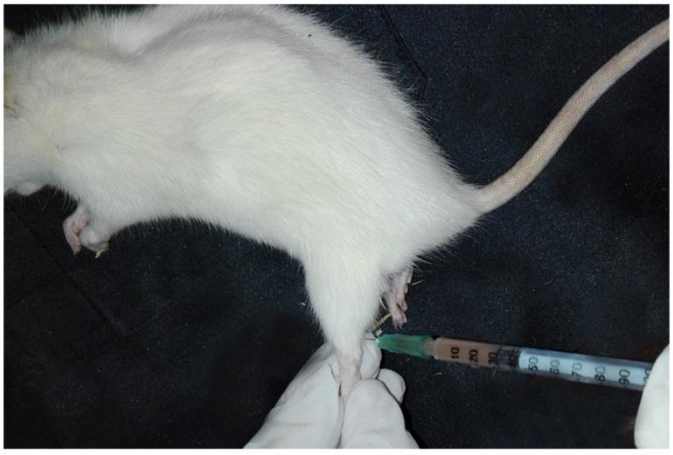

Fig. 1 Photograph showing Chitosan solution injection at the induced fracture site of rat tibia.

Fig. 2 Photograph showing cast application after Chitosan solution injection.

For radiological evaluation, Tibiae lateral views were taken by the Faxitron Cabinet X-ray System (Hewlett-Packard, 50 µm x-ray beam output; model 43855A; IL 60089, USA). High-resolution 30x40 cm films (Fuji HR-E 30 Medical X-ray) were used and radiations at 48 kVp and 15 mAs, at a 70 cm focal film distance (F.F.D.) were done at 7 days, 14 days and 28 days after fracture induction. The description and evaluation of the fracture healing (fracture gap and callus formation) was performed for all rats according to (Risselada et al., 2005).

Diagnostic ultra-sonographic machine (Mindray dp 10 Germany vet with multiple elements convex probe and a 7.5 MHz frequency), used to follow up the healing process with the aid of coupling gel to avoid air buckets after removal of casting tape were done at 7 days, 14 days and 28 days after fracture induction (Risselada et al., 2005).

The shafts of tibiae were harvested from rats were done at 7 days, 14 days and 28 days after fracture induction, removing the surrounding attached musculature, the bone specimens were then fixed in 10 % neutral buffered formalin for 48 hours. After fixation, bone were decalcified using a buffer solution of 17 % EDTA disodium solution (Ethylenediamine tetra-Acetic acid disodium salt B.P.93®: El Nasr pharmaceutical chemical, Egypt) for one month during which the specimens weekly inspected for signs of complete decalcification, as well as EDTA solution changed weekly if it was supersaturated with the released calcium (Shibata et al., 2000**).**

After complete decalcification, the bone specimens were washed in running tap water for 24 hours, then dehydrated in ascending grades of ethyl alcohol (70 %, 80 %, 90 % and 96 %) (Absolute 1, Absolute 2 and Absolute 3), cleared in xylene (xylene 1, xylene 2 and xylene 3) and embedded in soft paraffin (paraffin 1, paraffin 2 and paraffin 3) then blocked in hard paraffin wax, sectioned 5-7 µ and stained with routinely Hematoxylin and Eosin according to **(**Bancroft, and Marilyn, 2008 and Fathy et al., 2017).

3. Results

Results of first week post fracture induction

By the end of first week, Radiography of tibiae of control group (CG); fracture line was clearly visible, the gap was clearly visible and radiolucent (Error! Reference source not found.3), while in chitosan group (CT G) fracture line was less visible with clear evidence of callus formation; the gap was less visible Error! Reference source not found.4). Ultrasonography of CG Error! Reference source not found.5), showed that the bone surface was irregular in outline. Hypo-echoic regions indicate the presence of a hematoma, and CTG (Error! Reference source not found.6) Showed that the fracture site is filled with tissue with a mixed hypoechogenic and anechogenic appearance. The callus has an inhomogeneous and irregular appearance with areas of hyperechogenicity indicating start of mineralization.

Fig. 3 Radiograph of CG after first week; X-ray shows a transvers fracture of the tibial shaft below the fibular junction fracture edges are clearly visible and radiolucent (arrow).

Fig. 4 Radiograph of CT G after first week; X-ray shows a transvers fracture of the tibial shaft below the fibular junction the gap between fracture edges is less radiolucent, radiograph shows periosteal new bone separated from underlying cortex by thin radiolucent line, increase in bone density (sclerosis) at fracture margins (arrow)

Fig. 5 Ultrasonography of CG after first week the bone surface was irregular in outline. Hypo-echoic regions indicate the presence of a hematoma.

Fig. 6 Ultrasonography of CT G after first week. The fracture site (arrow) is filled with tissue with a mixed hypo-echogenic and an-echogenic appearance. The callus has an inhomogeneous and irregular appearance with areas of hyper-echogenicity indicating start of mineralization.

By gross pathological examination of the induced fractured site in the tibia shaft after one week for both CG and CTG injected group; the CG showed prominent inflammatory edema around the fracture site Fig. (7), while in CTG, this inflammatory edema was much lesser Fig. (8).

By the histopathological examination, the CG showing the end of the inflammatory phase where remnant granulation tissue filling the fracture gap which was rich with blood capillaries**,** and entangling in it lymphocytes**,** while bone fragments are still present in the site of the induced fracture Fig. (9), the CTG showing remnant of bone fragments due to the induction of the fracture, while there are active small blood capillaries filling the fractured gap Fig. (10).

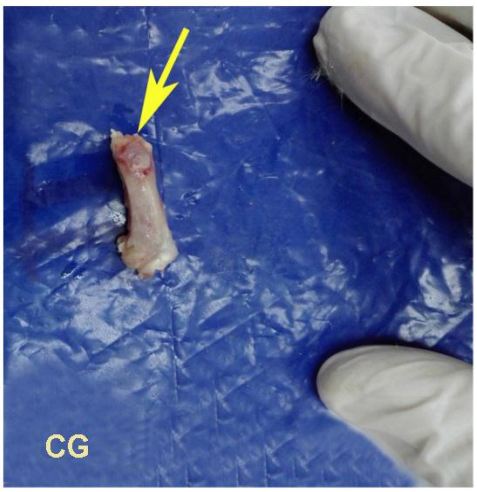

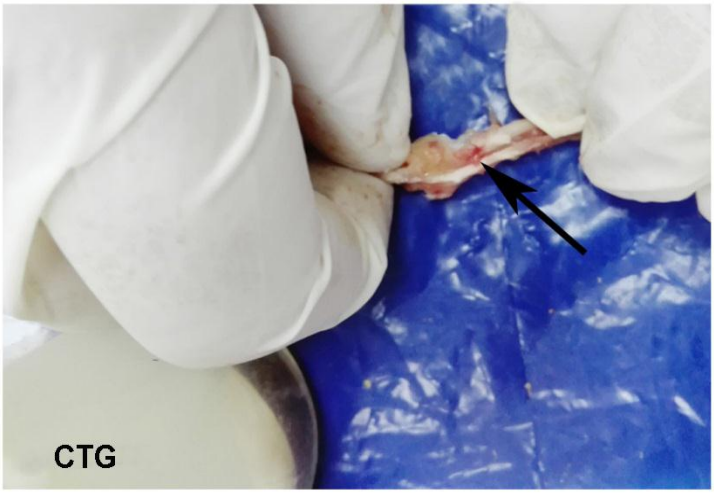

Fig. 7 Photograph of rat tibia of CG post fracture by one week showing inflammatory red zone at fracture site (yellow arrow).	Fig. 8 Photograph of tibia shaft after being harvested from the rat of CTG post fracture by one week showing minimal inflammatory area at the fracture site (black arrow).

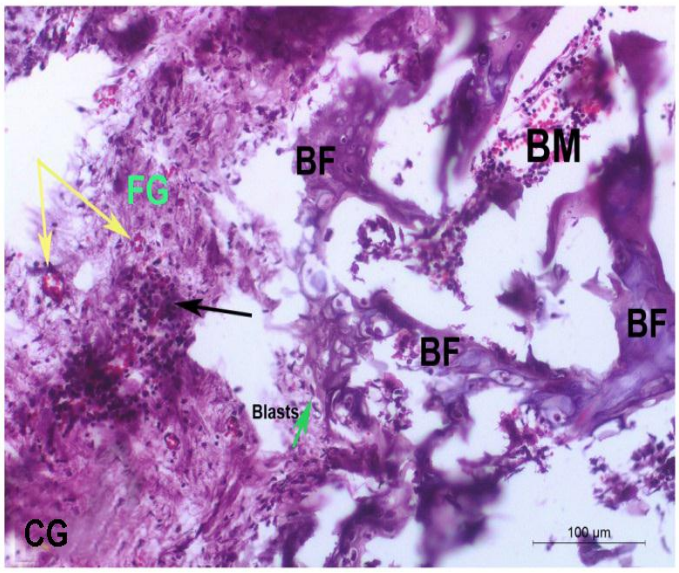

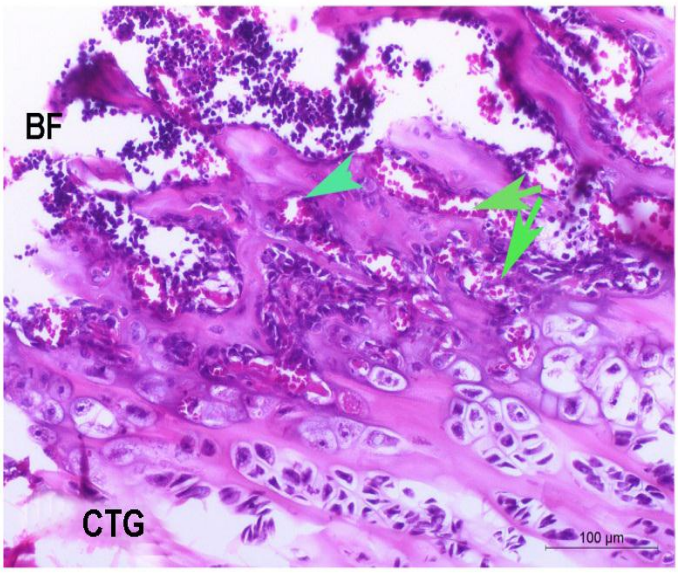

Results of Second week post fracture induction

In the second week, on radiography, revealed the appearance of peripheral callus and little bone bridges, whereas the gap between fracture edges is still visible in CG (**Error! Reference source not found.**), while in CTG fracture line start to disappear and callus formation was visible, fracture gap tend to be radiopaque. Meanwhile, on ultrasonography a global formation is evident related to the periosteal collars that tend to meet from the two sides of the fracture filling the gap. Hyper-echoic lines of tibia; in-betweens (fractured area) appeared as gray pitched hypo-echoic small gape denotes start of callus formation in CG (**Error! Reference source not found.**) and CTG (**Error! Reference source not found.**) with more extent (**Error! Reference source not found.**).

	
Fig.11 Radiograph of CG after second week fracture edges is still visible X-ray shows a transvers fracture of the tibial shaft below the fibular junction	Fig.12 Radiograph of CTG after second week X-ray shows a transvers fracture of the tibial shaft below the fibular junction the x-ray showed greater amount of calcification of callus than control group

Fig. 9 Photomicrograph of rat tibia of CG post fracture by one week showing granulation tissue filling fracture gap (FG), rich by blood capillaries (two yellow arrows), and entangling in it lymphocytes representing the end of the inflammatory phase of the fracture (black arrow), while bone fragment (BF) Bone marrow (BM) (H&E; Bar= 100 µm).	Fig. 10 Photomicrograph of rat tibia of CTG post fracture by one week showing remnant of small bone fragments (BF) associated with active blood capillaries in the fractured gap (green arrows) (H&E; Bar= 100 µm).

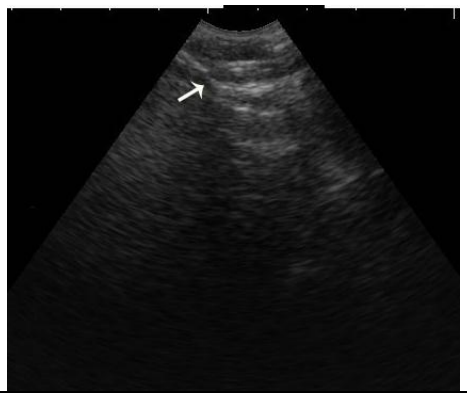	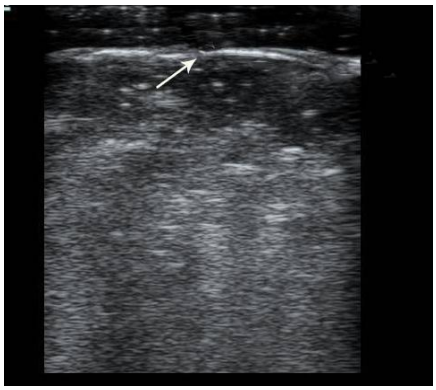
Fig. 13 Ultrasonogram of CG after second week, Hyper-echoic lines denote fractured bones; in-betweens gray pitched hypo-echoic small gape denotes start of callus formation	Fig. 14 Ultrasonogram of CTG after second week showed that Note the presence of reflective, irregular interfaces within the osteotomy gap indicative of bone production

By gross pathological examination of the induced fractured site in the tibia shaft after two weeks for both CG and CTG; the two groups showed hard callus formation Fig. (15) and Fig. (16).

By histopathological examination, the CG showed overfilling of the fractured gap with active fibrocytes, associated with active oesteoblasts as main structure of hard callus while all area of the fracture was clear from any erythrocytes and inflammatory cells Fig. (17). In the CTG, there was reduced gap between the two bony edges in which there is an active oesteoblasts associated with fibrocytes Fig. (18).

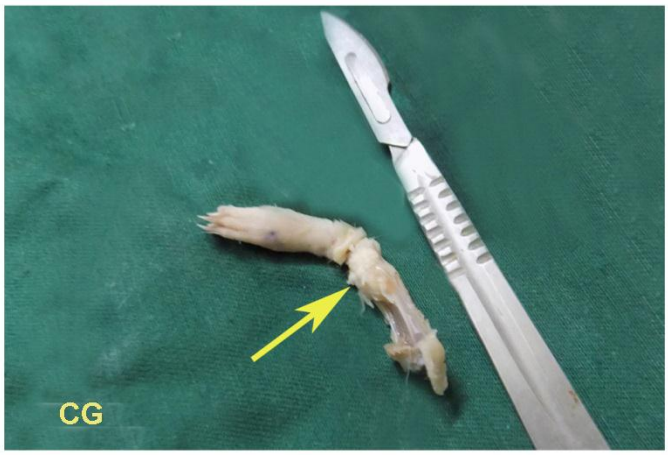

Fig. 15: Photograph of rat tibia of CG post fracture by two weeks showing beginning of formation of hard callus at fracture site (yellow arrow).	Fig. 16 Photograph of rat tibia of CTG post fracture by two weeks showing formation of hard callus at fracture site (black arrow).

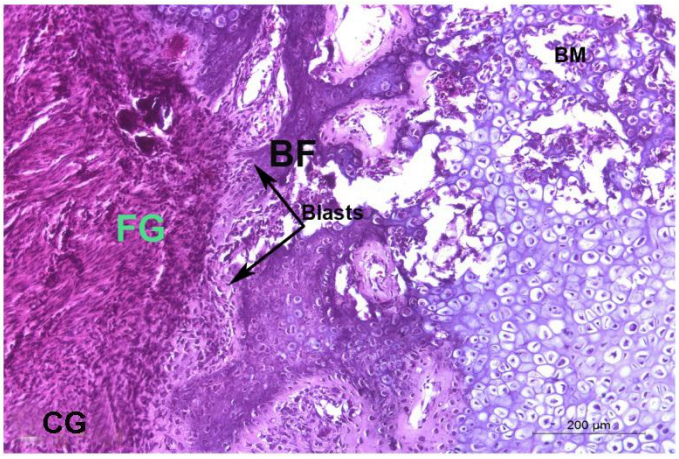

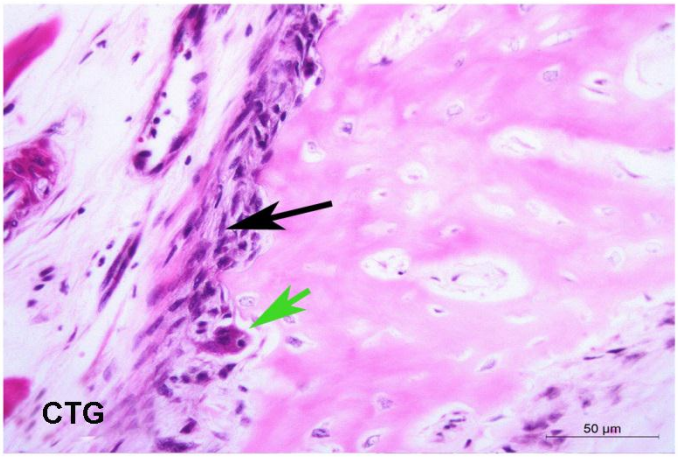

Fig. 17 Photomicrograph of rat tibia of CT post fracture by two weeks showing overfilling of the fractured gap by active fibrocytes, associated with active oesteoblasts (two black arrow) (H&E; Bar= 200 µm).	Fig. 18 Photomicrograph of rat tibia of CTG post fracture by two weeks showing active oesteoblasts and minimal fibrocytes (black arrow) associated with appearance of osteoclasts (green arrow) (H&E; Bar= 50 µm).

Results of Fourth week post fracture induction

In the fourth week, Radiography revealed the bone trabeculae extend from one fragment to the other, the solution of continuity dissolves, and the callus formation is completed. Fracture line is barely visible; callus bridges the fracture edges and the area in between become radiopaque Fig.). in CG, while in CTG callus is clearly visible and condensed with incomplete disappearance of fracture line Fig.), Meanwhile, On ultrasonography the echo reflected by the focus increases in intensity according to the initial callus calcification; the collars meet in one hyper-echogenic convex, bridge-shaped structure on the fracture gap. The hyper-echogenic structure represents a clear obstacle to the ultrasounds, and an acoustic shadow appears below the newly formed periosteal callus according to its progressive calcification. Hyper-echoic lines tibia; at the fractured area, appeared as pitched hyper echoic denotes incomplete callus bridging in CG (**Error! Reference source not found.**) and in CTG, the fractured area appeared as hyper echoic area revealed condense callus formation; hypo echoic fracture line nearly invisible (**Error! Reference source not found.**)**Error! Reference source not found.**

Fig.19 Radiograph of CG X-ray shows a transvers fracture of the tibial shaft below the fibular junction after fourth week remodeling not complete

Fig. 20 Radiograph of CTG X-ray shows a transvers fracture of the tibial shaft below the fibular junction after fourth week Almost complete bridging of the fracture ends with extensive bony deposition compared to that of control group

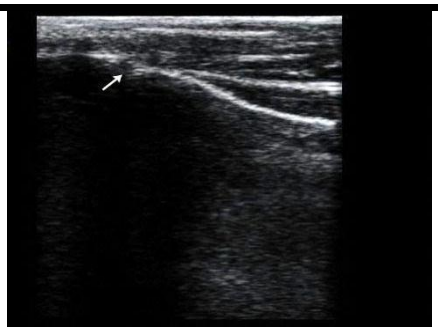

Fig. 21 Ultrasonogram of CG after fourth week, Hyper-echoic lines denote fractured bones; in-betweens pitched hyper echoic denotes incomplete callus bridging

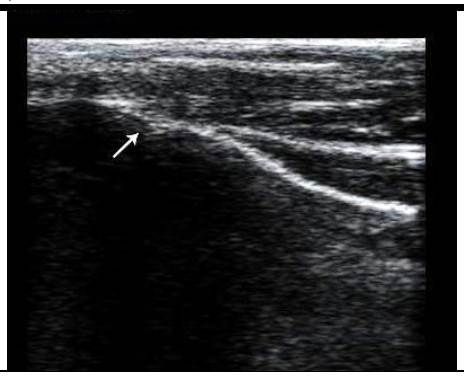

Fig. 22 Ultrasonogram of CTG after fourth week the bony surface is smoothly delineated, regular and homogeneously hyper echoic

By histopathological examination of the induced fractured site in the tibiae shaft after four weeks for both CG and CTG; the CG showed an area of organization represented by fibrocytes associated with active proliferation of fibers filling the fracture gap represent hard callus phase of bone healing Fig. (23), while in the CTG, the site of the fracture showed active oesteoblasts for the remodeling phase with minimal fibrocytes remained from the previous hard callus formation phase Fig. (24).

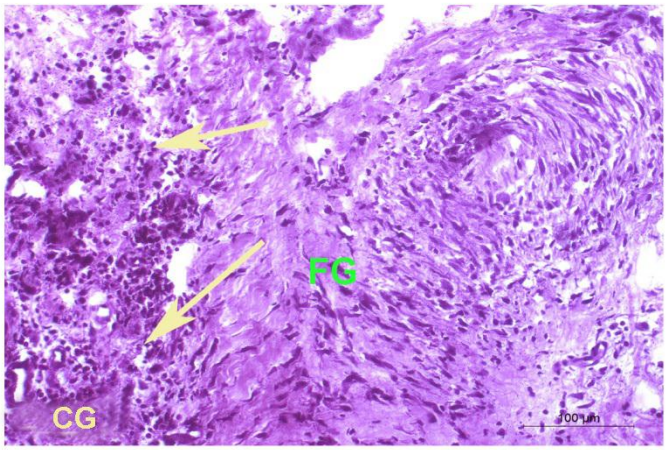

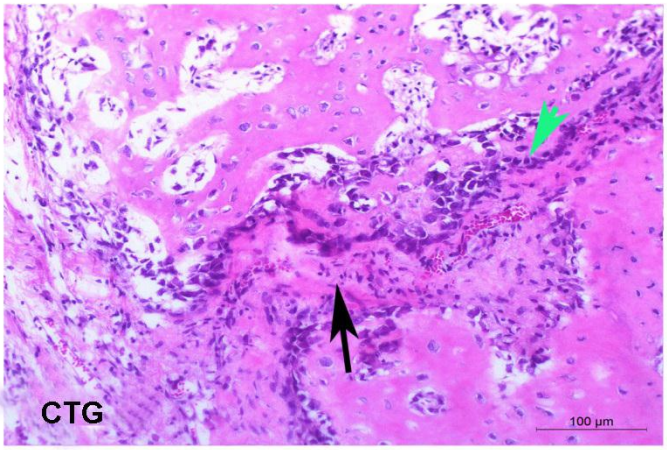

Fig. 23 Photomicrograph of rat tibia of CG post fracture by four weeks showing organization of fibrocytes (yellow arrows) associated with active proliferation of fibers filling fractured gap (green), (H&E; Bar= 100 µm).

Fig. 24 Photomicrograph of rat tibia of CTG post fracture by four weeks showing tissue resembling bone (black arrow), while osteoblasts penetrating the area (green arrow), (H&E; Bar= 100 µm).

4. Discussion

Results of the current study supported the hypothesis that assumed that chitosan enhance bone fracture healing when injected at site of fracture. Disappearance of fracture line, early callus formation, strong condensation of newly formed bone and early relieve of clinical signs were enhanced by injection chitosan in site of fracture during treatment. Statistical analysis proved presence of significant differences between healing in control and chitosan groups.

The major advantage of the external fixator is that it is fixed to the bone at some distance from the osteotomy and thus does not directly interfere with the healing process. Furthermore, the external fixator is easily removed post mortem (Haffner-Luntzer et al., 2016).

X-ray assessment is the most common clinical tool to assess hard tissue repair although this assessment is limited by its relatively qualitative nature (Axelrad and Einhorn, 2011) presents series of plain-film X-ray assessments made across a time course of fracture healing. Several radiographic features are easily observed during indirect or secondary fracture healing with the production of an external callus, these being the formation and growth of a calcified callus and the bridging of the fracture with callus (Spencer 1987, Oni et al. 1991, and Eastaugh-Waring et al., 2009).

As ultrasound can visualize developing callus even before radiographic changes are evident, it can therefore be utilized to assess the changes of bone healing (Craig et al., 1999). The presence of a hyperechoic ultrasound signal from the fracture sight was found to have a 100 percent correlation with the presence of hard fracture callus biopsy tissue (Moed et al., 1998).

In our study high effectiveness of ultrasound examination in evaluation of bone healing was proved. There were many advantages as lack of ionizing radiation, possibility of muscle visualization and qualitative assessment of the callus based on vascularization. The procedure was painless and well tolerated. The examination was easy to perform. Unfortunately we can perform the examination after plaster removal due to opacity of ultrasonic waves.

The current study found that chitosan had enhanced bone healing in terms of early callus formation and onset of remodeling.

Several studies have investigated various effects of chitosan on bone healing and raised some hypotheses on its mechanisms (Ueno et al., 2001 and Mizuno et al., 2003). According to a study by Chevrier and co-workers, chitosan increases the vascularization of blood vessels and stimulates budding tissue (tissue comprising of budding capillaries and fibroblasts (Chevrier et al., 2007). Park et al. (2000) reported that spongy chitosan activates osteoblasts and could increase osteogenesis. Bone tissue engineering, consists in the use of scaffolding. Vasconcelos et al. (2018b) suggested that chitosan scaffolds embedded with resolving D1 were able to lead to the formation of new bone with improvement of trabecular thickness. They observed an increase in new bone formation, in bone trabecular thickness, and in collagen type I and Coll I/ Coll III ratio.

This study showed augmentation of the production and thickness of new trabecular bone in the bone defect site. Thus, implantation of chitosan improved bone healing by raising the quantity and quality of trabecular bone.

Nonetheless, no effective drug has been developed for treating bone fractures so far. The present results indicate the potential of chitosan for therapy of bone defects and fractures.

References

Almeida, C. R., Serra, T., Oliveira, M. I., Planell, J. A., Barbosa, M. A. & Navarro, M. (2014). Impact of 3-D printed PLA- and chitosan-based scaffolds on human monocyte/macrophage responses: Unraveling the effect of 3-D structures on inflammation. Acta Biomaterialia, 10**,** 613-622.

Axelrad, T. W. & Einhorn, T. A. (2011). Use of clinical assessment tools in the evaluation of fracture healing. Injury, 42**,** 301-5.

Bancroft, J. D. and Marilyn, G. (2008). Theory and practice of histological techquines. 6th edition, North Hollywood, CA .USA.

Caruso, G., Lagalla, R., Derchi, L., Iovane, A. & Sanfilippo, A. (2000). Monitoring of fracture calluses with color Doppler sonography. Journal of clinical ultrasound, 28**,** 20-27.

Castillo, R. C., Bosse, M. J., Mackenzie, E. J., Patterson, B. M. & Group, L. S. (2005). Impact of smoking on fracture healing and risk of complications in limb-threatening open tibia fractures. Journal of orthopaedic trauma, 19**,** 151-157.

Chevrier, A., Hoemann, C., Sun, J. & Buschmann, M. 2007. Chitosan–glycerol phosphate/blood implants increase cell recruitment, transient vascularization and subchondral bone remodeling in drilled cartilage defects. Osteoarthritis and Cartilage, 15**,** 316-327.

Craig, J. G., Jacobson, J. A. & Moed, B. R. (1999). Ultrasound of fracture and bone healing. Radiol Clin North Am, 37**,** 737-51, ix.

Davis, B. J., Roberts, P. J., Moorcroft, C. I., Brown, M. F., Thomas, P. B. M. & Wade, R. H. (2004). Reliability of radiographs in defining union of internally fixed fractures. Injury, 35**,** 557-561.

Eastaugh-Waring, S. J., Joslin, C. C., Hardy, J. R. W. & Cunningham, J. L. (2009). Quantification of Fracture Healing from Radiographs Using the Maximum Callus Index. Clinical Orthopaedics and Related Research, 467**,** 1986-1991.

Elsisy, M., Elhamshary, A., Haroon, Y. M. & Sallam, S. (2014). Effect of chitosan on bone restoration in nasal bone defect: An experimental study. The Egyptian Journal of Otolaryngology, 30**,** 94.

Ezoddini-Ardakani, F., Azam, A. N., Yassaei, S., Fatehi, F. & Rouhi, G. (2011). Effects of chitosan on dental bone repair. Health, 3**,** 200.

Fathy M.Z., G.H. Ragab, M.M. Seif, S.M. Gadallah, Salah Deeb, Nesreen M. Safwat (2018). Clinico-radiographic and histopathologic evaluation of iliac shaft fracture in dogs (An experimental study). Beni-Suef University Journal of Basic and Applied Sciences 7 (2018) 165–170.

Flecknell, P. 2015. Laboratory animal anaesthesia, Academic press.

Giannoudis, P., Psarakis, S. & Kontakis, G. (2007). Can we accelerate fracture healing?: A critical analysis of the literature. Injury, 38**,** S81-S89.

Haffner-Luntzer, M., Kovtun, A., Rapp, A. E. & Ignatius, A. (2016). Mouse Models in Bone Fracture Healing Research. Current Molecular Biology Reports, 2.

Handool, K. O., Ibrahim, S. M., Kaka, U., Omar, M. A., Abu, J., Yusoff, M. S. M. & Yusof, L. M. (2018). Optimization of a closed rat tibial fracture model. Journal of experimental orthopaedics, 5**,** 13-13.

Ho, M.-H., Yao, C.-J., Liao, M.-H., Lin, P.-I., Liu, S.-H. & Chen, R.-M. (2015). Chitosan nanofiber scaffold improves bone healing via stimulating trabecular bone production due to upregulation of the Runx2/osteocalcin/alkaline phosphatase signaling pathway. International journal of nanomedicine, 10**,** 5941-5954.

Hohlbaum, K., Bert, B., Dietze, S., Palme, R., Fink, H. & Thöne-Reineke, C. 2018. Impact of repeated anesthesia with ketamine and xylazine on the well-being of C57BL/6JRj mice. PLOS ONE, 13**,** e0203559.

Jellouli, K., Bayoudh, A., Manni, L., Agrebi, R. & Nasri, M. (2008). Purification, biochemical and molecular characterization of a metalloprotease from Pseudomonas aeruginosa MN7 grown on shrimp wastes. Applied microbiology and biotechnology, 79**,** 989.

Kmiec, M., Pighinelli, L., Tedesco, M., Silva, M. & Reis, V. (2017). Chitosan-properties and applications in dentistry. Adv Tissue Eng Regen Med Open Access, 2**,** 00035.

Levengood, S. K. L. & Zhang, M. (2014). Chitosan-based scaffolds for bone tissue engineering. Journal of Materials Chemistry B, 2**,** 3161-3184.

Malafaya, P. B., Silva, G. A. & Reis, R. L. (2007). Natural-origin polymers as carriers and scaffolds for biomolecules and cell delivery in tissue engineering applications. Adv Drug Deliv Rev, 59**,** 207-33.

Mizuno, K., Yamamura, K., Yano, K., Osada, T., Saeki, S., Takimoto, N., Sakurai, T. & Nimura, Y. (2003). Effect of chitosan film containing basic fibroblast growth factor on wound healing in genetically diabetic mice. Journal of Biomedical Materials Research Part A: An Official Journal of The Society for Biomaterials, The Japanese Society for Biomaterials, and The Australian Society for Biomaterials and the Korean Society for Biomaterials, 64**,** 177-181.

Moed, B. R., Kim, E. C., Van Holsbeeck, M., Schaffler, M. B., Subramanian, S., Bouffard, J. A. & Craig, J. G. (1998). Ultrasound for the early diagnosis of tibial fracture healing after static interlocked nailing without reaming: histologic correlation using a canine model. J Orthop Trauma, 12**,** 200-5.

Oni, O. O., Dunning, J., Mobbs, R. J. & Gregg, P. J. (1991). Clinical factors and the size of the external callus in tibial shaft fractures. Clin Orthop Relat Res**,** 278-83.

Park, Y. J., Lee, Y. M., Park, S. N., Sheen, S. Y., Chung, C. P. & Lee, S. J. (2000). Platelet derived growth factor releasing chitosan sponge for periodontal bone regeneration. Biomaterials, 21**,** 153-159.

Prodinger, P. M., Foehr, P., Burklein, D., Bissinger, O., Pilge, H., Kreutzer, K., Von Eisenhart-Rothe, R. & Tischer, T. (2018). Whole bone testing in small animals: systematic characterization of the mechanical properties of different rodent bones available for rat fracture models. European Journal of Medical Research, 23**,** 8.

Risselada, M., Kramer, M., De Rooster, H., Taeymans, O., Verleyen, P. & Van Bree, H. (2005). Ultrasonographic and Radiographic Assessment of Uncomplicated Secondary Fracture Healing of Long Bones in Dogs and Cats. Veterinary Surgery, 34**,** 99-107.

Ruijin, Y., Hongsheng, L., Yizeng, X., Deyu, Y., Zaiquan, S. & Chunling, Y. (2016). Water-Soluble Chitosan Enhances Bone Fracture Healing in Rabbit Model. Current Signal Transduction Therapy, 11**,** 28-32.

Shibata, Y., Fujita, S., Takahashi, H., Yamaguchi, A. and Koji, T. (2000). Assessment of decalcifying protocols for detection of specific RNA by non-radioactive site hybridization in calcified tissue.Histochem. Cell Biol.: 113:153-159

Spencer, R. F. (1987). The effect of head injury on fracture healing. A quantitative assessment. J Bone Joint Surg Br, 69**,** 525-8.

Spin-Neto, R., De Freitas, R. M., Pavone, C., Cardoso, M. B., Campana-Filho, S. P., Marcantonio, R. A. C. & Marcantonio Jr, E. (2010). Histological evaluation of chitosan-based biomaterials used for the correction of critical size defects in rat's calvaria. Journal of Biomedical Materials Research Part A: An Official Journal of The Society for Biomaterials, The Japanese Society for Biomaterials, and The Australian Society for Biomaterials and the Korean Society for Biomaterials, 93**,** 107-114.

Tatari, H., Fidan, M., Erbil, G., Koyuncuoglu, M., Karci, T., Destan, H. & Tekmen, I. (2007). A new device to produce a standardized experimental fracture in the rat tibia. Saudi medical journal, 28**,** 866-871.

Ueno, H., Murakami, M., Okumura, M., Kadosawa, T., Uede, T. & Fujinaga, T. (2001). Chitosan accelerates the production of osteopontin from polymorphonuclear leukocytes. Biomaterials, 22**,** 1667-1673.

Vasconcelos, D. P., Costa, M., Neves, N., Teixeira, J. H., Vasconcelos, D. M., Santos, S. G., Aguas, A. P., Barbosa, M. A. & Barbosa, J. N. (2018a). Chitosan porous 3D scaffolds embedded with resolvin D1 to improve in vivo bone healing. J Biomed Mater Res A, 106**,** 1626-1633.

Vasconcelos, D. P., Costa, M., Neves, N., Teixeira, J. H., Vasconcelos, D. M., Santos, S. G., Águas, A. P., Barbosa, M. A. & Barbosa, J. N. (2018b). Chitosan porous 3D scaffolds embedded with resolvin D1 to improve in vivo bone healing. Journal of Biomedical Materials Research Part A, 106**,** 1626-1633.